

Comparative Study of Si-Ge-Sn Resonant Cavity Enhanced Heterojunction Bipolar Phototransistor under Quantum Confined Stark Effect and Franz Keldysh Effect at 1.55 μm

Soumava Ghosh

Institute of Radio Physics and Electronics, 92 A. P. C Road, Kolkata-700009

Abstract

Group-IV and their alloy based Heterojunction Bipolar Phototransistors (HPTs) are of immense interest in recent day optical communication. In this paper first resonant cavity enhanced heterojunction bipolar phototransistor (RCE-HPT) with $\text{Ge}_{0.992}\text{Sn}_{0.008}/\text{Si}_{0.30}\text{Ge}_{0.61}\text{Sn}_{0.09}$ Quantum Well/barrier structure under Quantum Confined Stark Effect (QCSE) has been evaluated. Further the bulk GeSn absorption region has been considered instead of QW/barrier structure and estimated the Franz Keldysh Effect (FKE). Finally different RCE-HPT related parameters such as quantum efficiency-bandwidth product, responsivity, collector current and optical gain have been studied and compared under QCSE and FKE.

Key Words: Franz Keldysh Effect, Quantum Confined Stark Effect, RCE HPT

Date of Submission: 02-02-2022

Date of Acceptance: 15-02-2022

I. Introduction

Over last few decades, optical communication has attracted new data hungry generation due to its low loss, low attenuation and high speed than conventional electronic communication. Among different active optical devices, photodetector (PD) is an important building block. In last few years a large number of researches have been done on PDs with III-V materials and their alloy. Although their performance is excellent in optical communication [1], but high fabrication cost has restricted their applications. Therefore, researchers have shifted their focus to alternative group-IV semiconductors. Si is an elementary group-IV semiconductor, but it is not compatible with modern optical communication window (1.3 μm and 1.55 μm), due to its bandgap energy i.e. 1.12eV [2]. This problem can be partially eradicated by using Ge, as its direct bandgap supports 1.55 μm at room temperature. But beyond 1.5 μm the optical response of Ge based devices falls drastically [3]. Therefore, entire optical telecommunication bands cannot be covered by them.

This scenario has been changed dramatically in last few decades after successful growth of high quality $\text{Ge}_{1-y}\text{Sn}_y$ films and SiGeSn alloys on Si substrate by practical chemical vapor deposition (CVD) [4,5] and molecular beam epitaxy (MBE) [6]. Beyond 8% Sn concentration the $\text{Ge}_{1-y}\text{Sn}_y$ alloy becomes a direct bandgap material [7] and further enhancement of Sn concentration reduces the bandgap and not only increases the absorption coefficient but also shows a red shift [8]. Based on those notable features researchers have developed different types of optical devices such as, light emitting diode [9], LASER [10,11], p-i-n PD [12-15], metal-semiconductor-metal PD (MSM PD) [16], avalanche photodiode (APD) [17], waveguide PD [18], quantum well infrared photodetector (QWIP) [19-22] and heterojunction bipolar phototransistor (HPT) [8, 23-27].

Among all those aforesaid PDs, HPT is a potential device. It is a strong competitor of p-i-n and APD due to its inherent gain and absence of excess noise. A number of researchers have reported the characteristics of HPT based on III-V compounds and their alloys [28-32] and group-IV compounds [23-27]. Basu et al. [23] have reported their study on HPT based on GeSn, which shows that GeSn based HPT can compete with InGaAs based devices.

Fidaner et al. [33] and Basu and Das [34] have reported the characteristics of photoconductors exploiting Quantum Confined Stark Effect (QCSE) and Franz-Keldysh Effect (FKE) respectively. Chang and Chang [35] have reported a strain free, type-I structure of $\text{Ge}_{0.992}\text{Sn}_{0.008}$ quantum well (QW) with $\text{Si}_{0.30}\text{Ge}_{0.61}\text{Sn}_{0.09}$ barrier. The lowest bandgap of QW is direct in nature reduces to 773.41 meV, which is lower than the bandgap of pure Ge. Chakraborty et al. [36] have shown resonant cavity enhanced (RCE) p-i-n PD, exploiting both FKE and QCSE. In our previous work [25] we have reported a comparison of HPT with and without resonant cavity. The RCE-HPT shows approximately eight times better response than conventional HPT with equal thickness of absorption layer. The multi pass of the light wave inside the device increases the

absorption in the active layer and thereby the optical response. These findings encourage the author for extending the study on RCE based HPT under QCSE and FKE and also comparing their performance at the recent telecommunication window i.e, 1.55 μm .

In this paper different RCE-HPT parameters exploiting FKE and QCSE such as Quantum Efficiency-Bandwidth Product (QEBWP), responsivity, terminal current, optical gain etc have been studied. The proposed structure exhibits in sec. 2, theoretical analysis part presents in sec. 3, followed by analytical results in sec. 4. Finally, the conclusion of this study presents in sec. 5.

II. Structure

In this study a *N-p-n* HPT with $100 \mu\text{m}^2$ cross-sectional area has been considered with normal biasing technique. The transverse electric (TE or x-y) polarized light incident on the emitter-base junction, i.e., front side illumination has been considered. Fig. 1 shows the proposed schematic HPT structure, which is grown on Si substrate via a fully strain-relaxed and lattice matched $\text{Si}_{0.30}\text{Ge}_{0.61}\text{Sn}_{0.09}$ buffer layer. The material compositions, doping concentrations, bandgap and dimensions of different regions are given in Table 1. 11 nm thick low bandgap $\text{Ge}_{0.992}\text{Sn}_{0.008}$ QW with 10 nm thick higher bandgap $\text{Si}_{0.30}\text{Ge}_{0.61}\text{Sn}_{0.09}$ barriers are used for absorption region, which is sandwiched between base and collector region. Higher bandgap *n*-type $\text{Si}_{0.34}\text{Ge}_{0.56}\text{Sn}_{0.10}$ has been considered as the emitter. The top and bottom mirror with reflectivity R_1 and R_2 have been used to create a vertical cavity effect. Under strong external electric field this structure shows QCSE phenomenon. On the other hand, if the absorption region is replaced by equal thickness i.e, 31 nm of bulk $\text{Ge}_{0.992}\text{Sn}_{0.008}$, in the presence of electric field it shows a strong FKE.

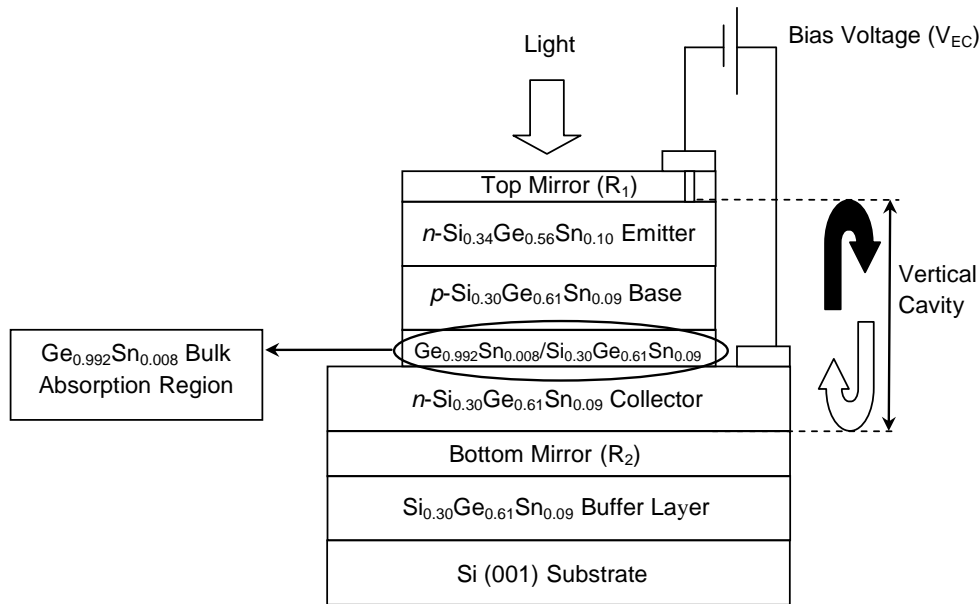


Fig. 1 Schematic diagram of front-side-illuminated SiGeSn HPT.

Table 1: Different parameters of SiGeSn HPT

Layer	Material	Band gap (eV)	Doping ($/\text{m}^3$)	Type	Width (nm)
Emitter	$\text{Si}_{0.34}\text{Ge}_{0.56}\text{Sn}_{0.10}$	0.9483	1×10^{23}	<i>N</i>	200
Base	$\text{Si}_{0.30}\text{Ge}_{0.61}\text{Sn}_{0.09}$	0.9144	2×10^{23}	<i>p</i>	200
Absorption Region	$\text{Ge}_{0.992}\text{Sn}_{0.008}$ (FKE)	0.6495	Undoped	-	31
	$\text{Ge}_{0.992}\text{Sn}_{0.008}/\text{Si}_{0.30}\text{Ge}_{0.61}\text{Sn}_{0.09}$ (QCSE)	0.6495 – QW 0.9144 – Barrier			11 – QW 10 – Barrier
Collector	$\text{Si}_{0.30}\text{Ge}_{0.61}\text{Sn}_{0.09}$	0.9144	5×10^{22}	<i>n</i>	500

III. Theoretical Modeling

In this section, the theoretical modeling of the proposed RCE-HPT, including the parameters related to absorption coefficient, quantum efficiency (QE), responsivity, bandwidth (BW), terminal current and optical gain are given. The parameters related to GeSn and SiGeSn alloys are obtained by linear interpolation of these of Si, Ge and Sn which can be found in Ref. [10].

3.1 Absorption Coefficient Calculation

Due to the physical phenomenon QCSE, the absorption coefficient may be expressed as [36],

$$\alpha(\hbar\omega) = \alpha_h \exp\left[-\frac{(\hbar\omega - \hbar\Omega_h)^2}{2(\hbar\Gamma_h)^2}\right] + \alpha_l \exp\left[-\frac{(\hbar\omega - \hbar\Omega_l)^2}{2(\hbar\Gamma_l)^2}\right] + \frac{\alpha_c}{1 + \exp\left(\frac{\hbar\Omega_c - \hbar\omega}{\hbar\Gamma_c}\right)} \times \frac{1}{1 + \exp\left\{2\pi[|\hbar\Omega_c - \hbar\omega|/R_y]^{-1/2}\right\}} \quad (1)$$

where, the optical energy is $\hbar\omega$, the excitonic peak energy is $\hbar\Omega$, Γ 's are the line width (HWHM), α 's represent the fitting parameters, R_y is the Rydberg's constant for exciton. The subscripts h, l and c denote heavy hole (HH), light hole (LH) and continuum states respectively.

For the bulk absorption region, the absorption coefficient due to FKE is given below [36],

$$\alpha(\hbar\omega) = \frac{\alpha_b}{(2\pi)^2} \left[\frac{2\mu_r}{\hbar^2}\right]^{3/2} (\hbar\omega - E_g)^{1/2} \times \left\{1 - \frac{E_0^{3/2}}{(\hbar\omega - E_g)^{3/2}} \cos\left\{\frac{4}{3}\left[\frac{(\hbar\omega - E_g)}{E_0}\right]^{3/2}\right\}\right\} \quad (2)$$

where, E_g , μ_r and E_0 stand for direct band gap energy, reduced mass and subband energy respectively.

By using the approach of model solid theory [37], the band gap energy E_g is obtained by [36],

$E_g = E_{dir} + \delta E_h^{cf}$ and $\delta E_h^{cf} = a_c \frac{\Delta\Omega}{\Omega}$ where a_c is the conduction band hydrostatic deformation potential and E_{dir} denote the direct band gap of the absorption region.

The sub band energy (E_0) and the absorption coefficient (α_b) depend on the external electric field F , are given below [36],

$$\alpha_b = \frac{2\pi\langle|p_{cv}|^2\rangle}{n\epsilon_0\omega c} \left(\frac{e}{m_0}\right)^2 \text{ and } E_0 = (e^2 F^2 \hbar^2 / 2\mu_r)^{1/3} \quad (3)$$

where, the momentum matrix is,

$$\langle|p_{cv}|^2\rangle = \frac{m_0^2 E_g (E_g + \Delta)}{3m_e (E_g + 2\Delta/3)} \quad (4)$$

Δ is the spin-orbit splitting and n is the refractive index (R.I.).

3.2 Photodetector parameters

For a conventional structure without any resonating cavity, the QE can be expressed as [25],

$$\eta_{\text{Conventional-HPT}} = (1 - R_1)(1 - e^{-\alpha d}) \quad (5)$$

where, α is the absorption coefficient, d is the active region thickness and R_1 is the reflectivity of the anti-reflection (AR) coating for reducing light reflection from the top surface of the HPT.

The QE of the resonant cavity structure is given as [25],

$$\eta_{\text{RCE-HPT}} = \frac{(1 + R_2 e^{-\alpha d})(1 - R_1)(1 - e^{-\alpha d})}{1 - 2\sqrt{R_1 R_2} e^{-\alpha d} \cos(2\beta L + \Psi_1 + \Psi_2) + R_1 R_2 e^{-2\alpha d}} \quad (6)$$

where, $\alpha(E,F)$ is the absorption coefficient at photon energy E and external electric field F , L is the cavity length, Ψ_1 and Ψ_2 are the phase shifts introduced by top and bottom mirror, and R_1 and R_2 are the front and back mirror reflectivity respectively. The propagation constant (β) is calculated by, $\beta = \frac{2\pi n}{\lambda}$, where λ is the wavelength and n is the R.I. As, the R.I. (n) changes to $(n + \Delta n)$, due to the linear electro optic effect, so the propagation constant (β) and QE (η) change according to the external electric field.

The BW of the PD depends on both RC and transit time delay components. As the active region is very thin, in this analysis the RC time delay can be neglected. Therefore, the BW can be calculated by using the relation [25],

$$f_{3\text{-dB}} = 0.45 \left(\frac{v}{d}\right) \quad (7)$$

where, v is the electron drift velocity [25],

$$v = \frac{\mu F}{\sqrt{1 + \left(\frac{\mu F}{v_s}\right)^2}} \quad (8)$$

where μ is the mobility and v_s is the electron saturation velocity. Since, till now the saturation velocity of GeSn alloy is unknown; therefore, in this analysis the saturation velocity of pure Ge i.e, 6×10^4 m/s has been considered [14]. As, GeSn alloy has higher carrier mobilities than pure Ge [38], the consideration of the value of saturation velocity of pure Ge may be true and reasonable.

The peak QE at resonant point, may be expressed as [39],

$$\eta_P = \left\{ \frac{(1 + R_2 e^{-\alpha d})}{(1 - \sqrt{R_1 R_2} e^{-\alpha d})^2} \right\} \times (1 - R_1) \times (1 - e^{-\alpha d}) \quad (9)$$

The base-collector junction responsivity can be calculated by [14],

$$\mathfrak{R} = \eta \left(\frac{e\lambda}{hc} \right) \quad (10)$$

3.3 HPT Modeling

The common emitter current gain is obtained by [24],

$$h_{FE} = \frac{\alpha}{1 - \alpha} = \frac{\gamma}{1 + \gamma \left[\cosh \left(\frac{W_B}{L_{nB}} \right) - 1 \right]} \quad (11)$$

where,

$$\gamma = \frac{\gamma_0 (\xi_1 / \xi_2)}{\sinh(W_B / L_{nB})} \quad (12)$$

and,

$$\gamma_0 = \frac{D_{nB} L_{pE} N_E}{D_{pE} L_{nB} N_B} \left(\frac{m_{nB}^* m_{pB}^*}{m_{nE}^* m_{pE}^*} \right) \exp \left(\frac{\Delta E_g}{k_B T} \right) \quad (13)$$

The responsivity of HPT can be calculated by [40],

$$\mathcal{R} = h_{FE} \times \mathfrak{R} \quad (14)$$

where h_{FE} is the common emitter current gain and \mathfrak{R} is the base-collector junction responsivity.

The enhancement factor (EF), which indicates the enhancement of the responsivity of the RCE-HPT than conventional one can be calculated by [15],

$$EF = \mathcal{R}_{RCE-HPT} / \mathcal{R}_{Conventional-HPT} \quad (15)$$

The collector current can be expressed as [25],

$$I_C = (1 + h_{FE}) (I_{ph} + I_{C0}) \quad (16)$$

where I_{C0} stands for the reverse saturation current, can be written as [25],

$$I_{C0} = eA \left[\frac{D_{pE}}{L_{pE}} p_{n0} + \frac{D_{nB}}{L_{nB}} n_{p0} \tanh \left(\frac{W_B}{L_{nB}} \right) \right] \quad (17)$$

where, D and L denote the diffusivity constant and diffusion length of the carrier, W is the thickness, A is the cross-sectional area, n_{p0} and p_{n0} are the minority carrier concentrations in the emitter and base under thermal equilibrium condition. The subscripts p, n, E and B stand for hole, electron, emitter and base respectively.

I_{ph} is the photocurrent, is obtained by [25],

$$I_{ph} = \mathfrak{R} \times P_{inc} \quad (18)$$

where P_{inc} is the incident photon power.

The optical gain (G) can be defined as [25],

$$G = (1 + h_{FE}) \times \eta \quad (19)$$

IV. Results and Discussions

With the help of eqn. (1) the absorption spectra in the presence of QCSE phenomenon has been evaluated. The different parameters regarding this calculation are taken from the Ref. [41]. When a bulk $Ge_{0.992}Sn_{0.008}$ absorption layer has been considered instead of GeSn/SiGeSn well-barrier structure, then a strong FKE has been noticed in the presence of external electric field. The absorption coefficient under FKE has been calculated by eqn. (2). Those values of absorption coefficients are used for QE and responsivity calculation.

The QEBWP has been calculated by using eqns. (6) and (7). The velocity of the electron in eqn. (7) is the drift velocity, which is a simplified assumption at high speed [25]. The responsivity of HPT has been estimated by eqn. (14). In fig. 2 and 3 we have plotted the QEBWP and HPT responsivity against optical frequency (wavelength). The variation of relative QE ($\Delta\eta/\eta$) as a function of optical frequency (wavelength), which has been evaluated from eqns. (6) and (9) is shown in fig. 4. By using eqn. (15) the EF has been calculated and plotted against optical frequency (wavelength) in fig. 5. Fig. 6 depicts the variation of the calculated collector current (I_C) measured by eqn. (16) with optical frequency (wavelength).

All the figures (fig. 2 to fig. 6) depict comparative studies of different parameters regarding HPT exploiting QCSE and FKE where the operating voltage is fixed at 2 MV/m. Those figures clearly exhibit that, the FKE based RCE-HPT show better response in lower optical frequency ranges of 178 - 192.8 THz on the other hand QCSE becomes dominating in 192.8 to 203 THz range.

The band gap of the bulk $Ge_{0.992}Sn_{0.008}$ is 0.74 eV which supports 1.68 μm (~178 THz) wavelength and therefore does not match with the recent optical communication window i.e., 1.55 μm . On the other hand, from those figures it has been noticed that at ~192.8 THz optical frequency which is equivalent to the 1.55 μm wavelength QCSE shows approximately three times better response than FKE based RCE-HPT. So we can say that at 1.55 μm QCSE based device is suitable than FKE.

By using eqns. (11) and (19) the small signal current gain and optical gain have been calculated respectively. From the fig. 7 it has been concluded that the enhancement of emitter width can not affect the small signal current gain and optical gain of HPT at fixed carrier density in emitter, ie, $N_E = 2 \times 10^{24} / m^3$. The fig.

8 shows the variation of the small signal current gain and optical gain with base width. When the base width increases then more number of injected carriers from the emitter are recombined inside the base before reaching to the collector. So automatically the gains reduce for a constant base concentration $N_B = 1 \times 10^{24} / m^3$.

Fig. 9 depicts the effect of emitter carrier concentration of the gain of the RCE-HPT under FKE and QCSE. In both the cases it has been found that enhancement of the carrier concentration inside the emitter region increases the density of the injected carriers towards the collector end through base. Therefore, the optical and small signal current gains increase with enhancement of the emitter concentration. On the other hand, when the carrier concentration of the base increases, most of the injected carriers from the emitter are recombined before reaching to the collector end. Thus, the optical and electrical responses diminish with enhancement of the base carrier concentration. This phenomenon is depicted in fig. 10. In those plots of gain variation against width and concentration of emitter and base regions, the operating wavelength is fixed at 1.55 μm .

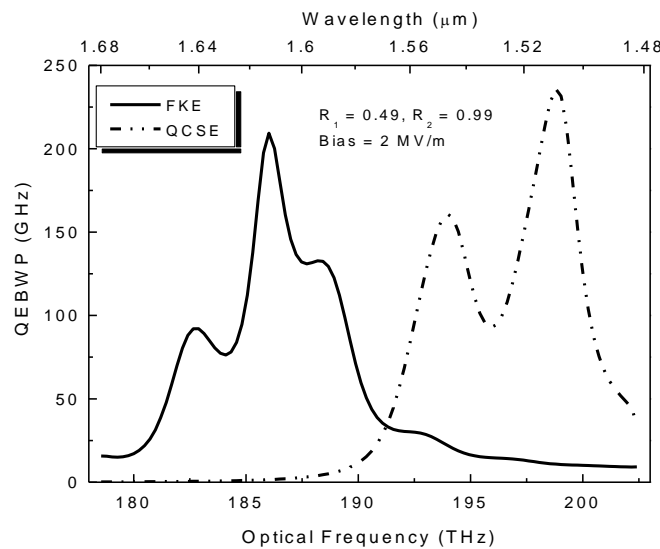


Fig. 2 QEBWP variation with Optical Frequency (Wavelength) for RCE-HPT.

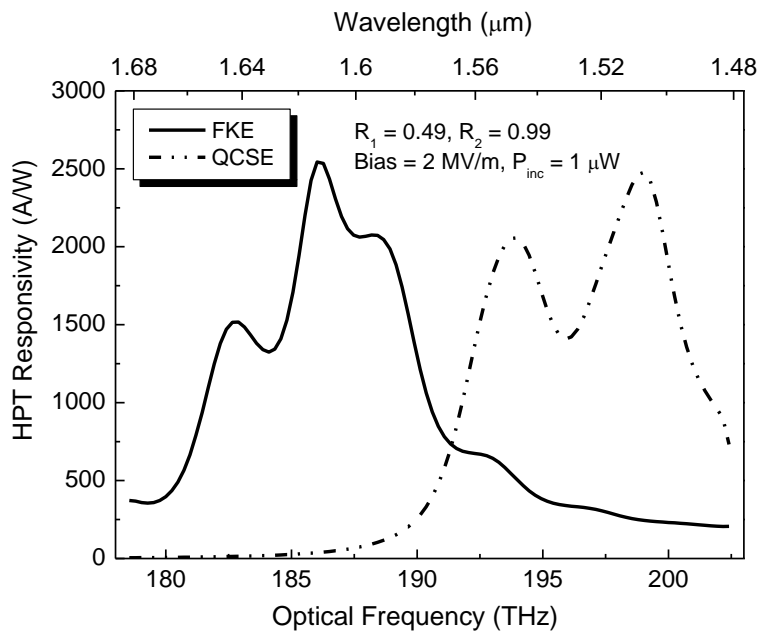


Fig. 3 Variation of HPT Responsivity with Optical Frequency (Wavelength) for RCE-HPT.

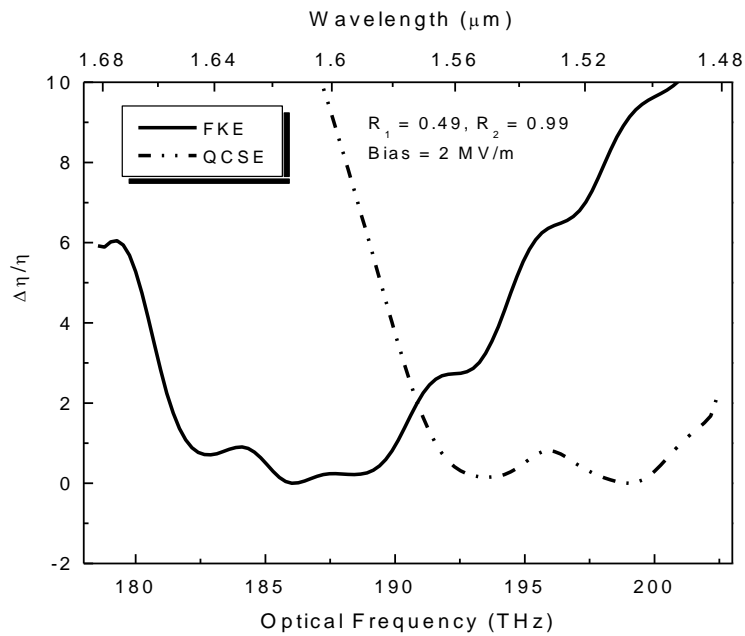


Fig. 4 Plot of $\Delta\eta/\eta$ with Optical Frequency (Wavelength) for RCE-HPT.

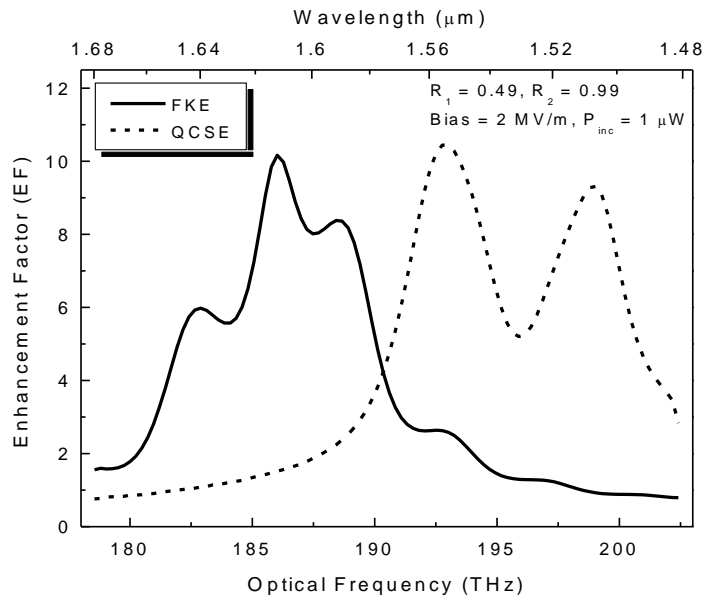


Fig. 5 Variation of Enhancement Factor against Optical Frequency (Wavelength) for RCE-HPT.

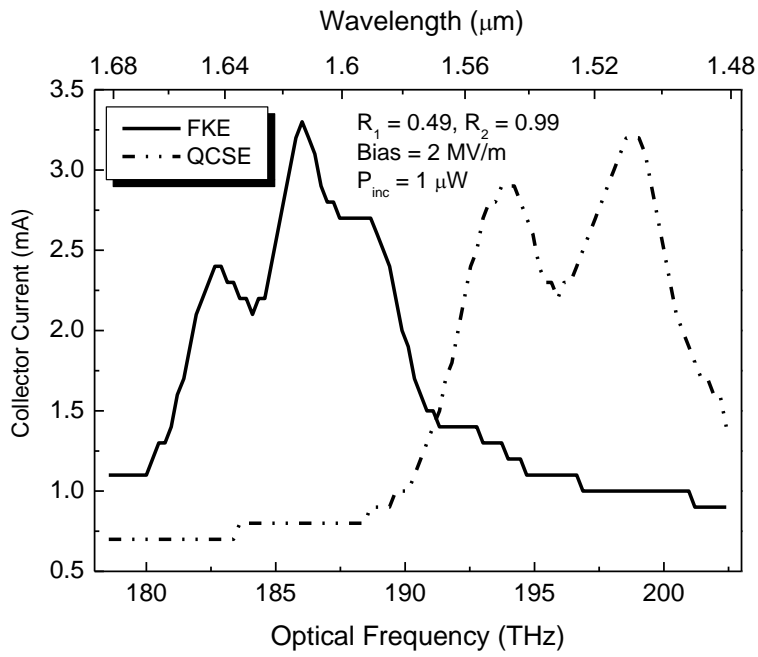


Fig. 6 Collector Current variation with Optical Frequency (Wavelength) for RCE-HPT.

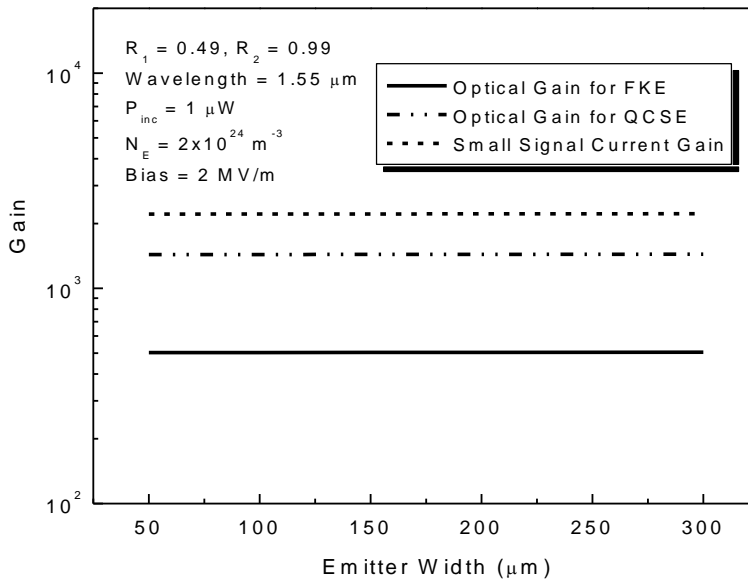


Fig. 7 Gain variation with Emitter Width for RCE-HPT.

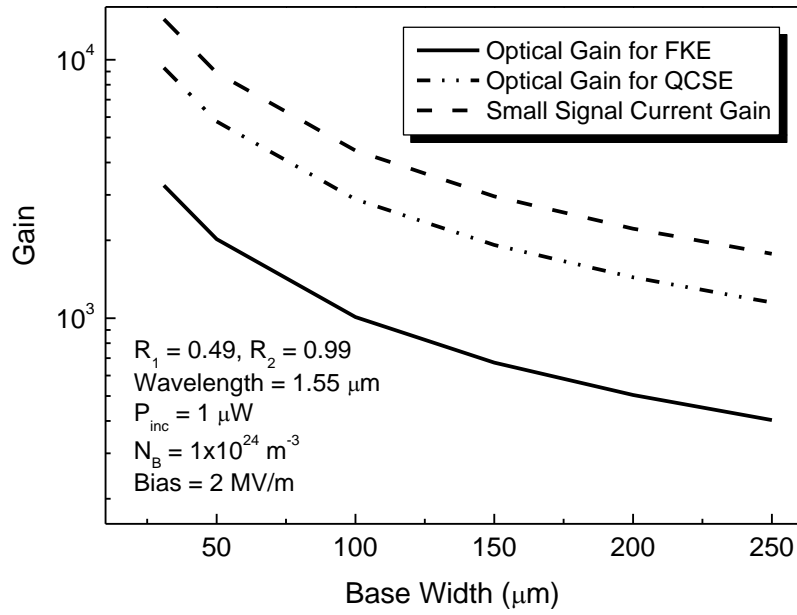


Fig. 8 Gain variation with Base Width for RCE-HPT.

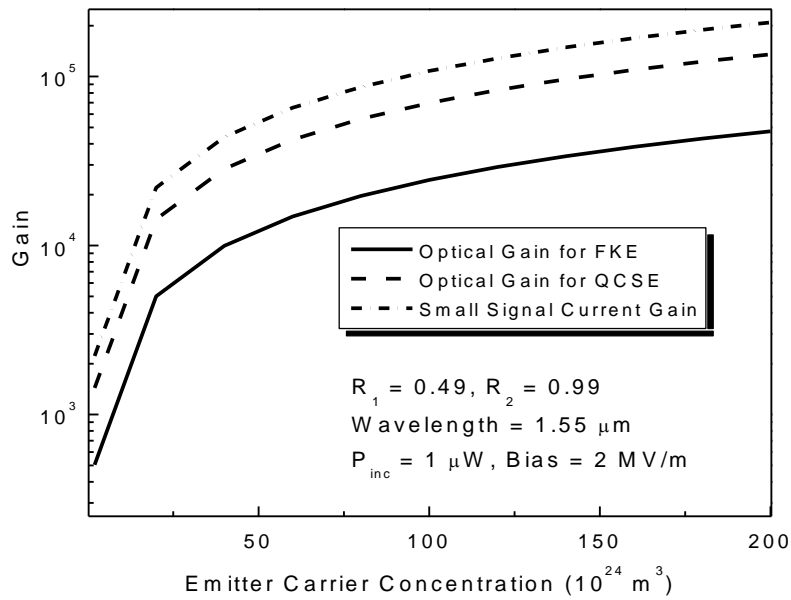


Fig. 9 Gain variation with Emitter Concentration for RCE-HPT.

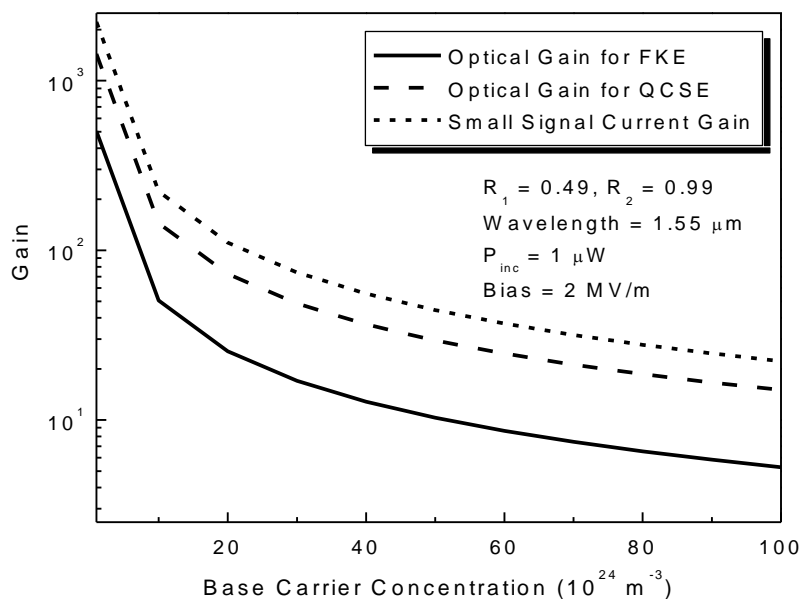


Fig. 10 Gain variation with Base Concentration for RCE-HPT.

V. Conclusion

From this study it has been noticed that, when the absorption region is considered the GeSn/SiGeSn well-barrier structure, the RCE-HPT shows a strong QCSE under external electric field. Again, when this structure has been replaced by equivalent thickness of bulk GeSn, due to the direct band gap nature and high absorption it shows FKE in the presence of electric field. In this study first different characteristics of RCE-HPT exploiting strong QCSE and FKE have been compared. After that at 1.55 μm the optical and small signal current gains have been evaluated as a function of width and carrier concentration of the base and emitter region. Although the band gap of the GeSn does not match with 1.55 μm but nevertheless at that wavelength QCSE based device gives approximately three times better response than FKE based RCE-HPT.

Acknowledgement

The author is thankful to Dr. Bratati Mukhopadhyay (Assistant Professor) and Dr. Gopa Sen (Professor) at Institute of Radio Physics and Electronics, University of Calcutta, Kolkata, India.

References

- [1]. R. W. M. Hoogeveen, R. J. van der A, and A. P. H. Goede: Extended wavelength InGaAs infrared (1.0–2.4 μm) detector arrays on SCIAMACHY for space-based spectrometry of the Earth atmosphere. [Journal] *Infr. Phys. Technol.* **42**, 1–16 (10.1016/S1350-4495(00)00061-X)
- [2]. M. J. Deen, P. K. Basu: Silicon Photonics: Fundamentals and Devices. [Book] Wiley, Chichester (2012)
- [3]. J. Michel, J. Liu, L. C. Kimmerlin: High performance Ge-on-Si Photodetectors. [Journal] *Nat. Photonics* **4**, 527-534 (10.1038/nphoton.2010.157)
- [4]. M. Bauer, J. Taraci, J. Tolle, A.V.G. Chizmeshya, S. Zollner, D.J. Smith, J. Menendez, C. Hu, J. Kouvetakis: Ge-Sn semiconductors for band-gap and lattice engineering. [Journal] *Appl. Phys. Lett.* **81**(1-3), 2992 (10.1063/1.1515133)
- [5]. A. V. G. Chizmeshya, C. Ritter, J. Tolle, C. Cook, J. Menendez, J. Kouvetakis: Fundamental studies of P(GeH₃)₃, As(GeH₃)₃, and Sb(GeH₃)₃: practical n-dopants for new group IV semiconductors. [Journal] *Chem. Mater.* **18**, 6266-6277 (2006)
- [6]. J. P. Gupta, N. Bhargava, S. Kim, T. Adam, and J. Kolodzey: Infrared electroluminescence from GeSn heterojunction diodes grown by molecular beam epitaxy. [Journal] *Appl. Phys. Lett.* **102**, 251117 (10.1063/1.4812747)
- [7]. B. Dutt, H. Lin, D. S. Sukhdeo, B. M. Vulovic, S. Gupta, D. Nam, K. C. Saraswat, J. S. Harris Jr.: Theoretical Analysis of GeSn Alloys as a Gain Medium for a Si-Compatible Laser. [Journal] *IEEE J. Sel. Top. Quant. Electron.* **19**, 1502706 (10.1109/JSTQE.2013.2241397)
- [8]. G. -E. Chang, R. Basu, B. Mukhopadhyay, and P. K. Basu: Design and modeling of GeSn-based heterojunction phototransistors for communication applications. [Journal] *IEEE J. Sel. Topics Quantum Electron.* **22**, 425–433 (10.1109/JSTQE.2016.2553447)
- [9]. M. Oehme, K. Kostecky, T. Arguirov, G. Mussler, K. Ye, M. Golhofer, M. Schmid, M. Kaschel, R. A. Körner, M. Kittler, et al.: GeSn Heterojunction LEDs on Si Substrates. [Journal] *IEEE Photon. Technol. Lett.* **26**, 187–189 (10.1109/LPT.2013.2291571)
- [10]. G. -E. Chang, S. -W. Chang, S. L. Chuang: Strain-Balanced Ge_zSn_{1-z}-Si_xGe_ySn_{1-x-y} Multiple-Quantum-Well Lasers. [Journal] *IEEE J. Quantum Electron.* **46**, 1813-1820 (10.1109/JQE.2010.2059000)

- [11]. S. Ghosh, B. Mukhopadhyay, G. Sen: Performance Enhancement of GeSn Transistor Laser with Symmetric and Asymmetric Multiple Quantum Well in the Base. [Journal] *Semiconductors* **54**, 77-84 (10.1134/S1063782620010212)
- [12]. S. Su, B. Cheng, C. Xue, W. Wang, et al.: GeSn p-i-n photodetector for all telecommunication band detection. [Journal] *Opt. Express* **19**, 6400-6405 (2011)
- [13]. M. Oehme, M. Schmid, M. Kaschel, M. Gollhofer, D. Widmann, E. Kasper, J. Schulze: GeSn p-i-n detectors integrated on Si with up to 4% Sn. [Journal] *Appl. Phys. Lett.* **101**, 141110 (10.1063/1.4757124)
- [14]. S. Ghosh, B. Mukhopadhyay, G. -E. Chang: Design and Analysis of GeSn-Based Resonant-Cavity-Enhanced Photodetectors for Optical Communication Applications. [Journal] *IEEE Sens. J.* **20**, 7801-7809 (10.1109/JSEN.2020.2981416)
- [15]. S. Ghosh, H. Kumar, B. Mukhopadhyay, G. -E. Chang: Design and Modeling of High-Performance DBR-Based Resonant-Cavity-Enhanced GeSn Photodetector for Fiber-Optic Telecommunication Networks. [Journal] *IEEE Sens. J.* **21**, 9900-9908 (10.1109/JSEN.2021.3054475)
- [16]. S. Ghosh, K. -C. Lin, C. -H. Tsai, H. Kumar, Q. Chen, L. Zhang, B. Son, C. S. Tan, M. Kim, B. Mukhopadhyay, and G. -E. Chang: Metal-Semiconductor-Metal GeSn Photodetectors on Silicon for Short-Wave Infrared Applications. [Journal] *Micromachines*, **11**, 795 (10.3390/mi11090795)
- [17]. Y. Dong, W. Wang, X. Xu, X. Gong, D. Lei, Q. Zhou, Z. Xu, W. Khai Loke, S. -F. Yoon, G. Liang, Y. -C. Yeo: Germanium-Tin on Si Avalanche Photodiode: Device Design and Technology Demonstration. [Journal] *IEEE Trans. Electron. Dev.* **62**, 128-135 (10.1109/ted.2014.2366205)
- [18]. Y. H. Peng, H. H. Cheng, V. I. Mashanov, G. -E. Chang: GeSn p-i-n waveguide photodetectors on silicon substrates. [Journal] *Appl. Phys. Lett.* **105**, 231109(1-4) (10.1063/1.4903881)
- [19]. P. Pareek, M. K. Das, S. Kumar: Responsivity Calculation of Group IV-based Interband MQWIP. [Journal] *J. Comput. Electronics* **17**, 319-328 (10.1007/s10825-017-1071-y)
- [20]. S. Ghosh, S. Dey, B. Mukhopadhyay, G. Sen: Study of High-Frequency Performance in GeSn-Based QWIP. [Conference] *7th International Conf. Computers and Devices for Communication*, 448-452 (10.1007/978-981-15-8366-7_66)
- [21]. S. Ghosh, B. Mukhopadhyay, G. Sen, P. K. Basu: Performance analysis of GeSn/SiGeSn Quantum Well Infrared Photodetector in Terahertz Wavelength Region. [Journal] *Phys. E: Low-dimensional Systems and Nanostructures* **115**, 113692 (10.1016/j.physe.2019.113692)
- [22]. S. Ghosh, A. Bhattacharyya, G. Sen, B. Mukhopadhyay: Optimization of different structural parameters of GeSn/SiGeSn Quantum Well Infrared Photodetector (QWIP) for low dark current and high responsivity. [Journal] *J. Comput. Electronics*, **20**, 1224-1233, (10.1007/s10825-021-01668-w)
- [23]. R. Basu, V. Chakraborty, B. Mukhopadhyay, P. K. Basu: Predicted performance of Ge/GeSn hetero-phototransistors on Si substrate at 1.55 μm . [Journal] *Opt. Quant. Electron.* **47**, 387-399 (10.1007/s11082-014-9921-3)
- [24]. V. Chakraborty, S. Dey, R. Basu, B. Mukhopadhyay, P. K. Basu: Current gain and external quantum efficiency modeling of GeSn based direct bandgap multiple quantum well heterojunction phototransistor. [Journal] *Opt. Quant. Electron.* **49**(1-13), 125 (10.1007/s11082-017-0947-1)
- [25]. S. Ghosh, B. Mukhopadhyay, G. Sen, P. K. Basu: Study of Si-Ge-Sn based Heterobipolar Phototransistor (HPT) exploiting Quantum Confined Stark Effect and Franz Keldysh effect with and without resonant cavity. [Journal] *Phys. E: Low-dimensional Systems and Nanostructures* **106**, 62-67 (10.1016/j.physe.2018.10.012)
- [26]. S. Ghosh, B. Mukhopadhyay, G. Sen, P. K. Basu: Analysis of Some Important Parameters of Si-Ge-Sn RCE-HPT Exploiting QCSE and FKE. [Conference] *In Proceedings of the URSI-RCRS*, (10.23919/URSIRCRS49211.2020.9113616)
- [27]. W. -T. Hung, D. Barshilia, R. Basu, H. H. Cheng, G. -E. Chang: Silicon-based High-responsivity GeSn Short-wave Infrared Heterojunction Phototransistors with a Floating Base. [Journal] *Opt. Lett.* **45**, 1088-1091 (2020)
- [28]. S. M. Frimel, K. P. Roenker: A thermionic-field-diffusion model for Npn bipolar heterojunction phototransistors. [Journal] *J. Appl. Phys.* **82**, 1427-1437 (10.1063/1.365920)
- [29]. S. M. Frimel, K. P. Roenker: Gummel-Poon model for Npn heterojunction bipolar phototransistor. [Journal] *J. Appl. Phys.* **82**, 3581-3592 (10.1063/1.365677)
- [30]. S. H. Tan, H. R. Clen, W. T. Chen, M. K. Hsu, A. H. Lin, W. S. Lour: Characterization and modeling of three-terminal heterojunction phototransistors using an InGaP layer for passivation. [Journal] *IEEE Trans. Electron. Dev.* **52**, 204-210 (2005)
- [31]. H. A. Khan, A. A. Rezazadeh, S. Sohaib: Modeling and analysis of the spectral response for AlGaAs/GaAs HPTs for short wavelength optical communication. [Journal] *J. Appl. Phys.* **109**, 104507 (10.1063/1.3585846)
- [32]. M. S. Park, J. H. Jang: Enhancement of optical gain in floating-base InGaP-GaAs heterojunction phototransistors. [Journal] *IEEE Photon. Technol. Lett.* **22**, 1202-1204 (2010)
- [33]. O. Fidaner, A.K. Okyay, J.E. Roth, et al.: Ge-SiGe quantum well waveguide photodetectors on silicon for the near-infrared. [Journal] *IEEE Photon. Technol. Lett.* **19**(20), 1631-1633 (10.1109/LPT.2007.904929)
- [34]. P. K. Basu, N. R. Das, et al.: Ge/Si photodetectors and group IV alloy based photodetector materials. [Journal] *Opt. Quant. Electron.* **41**, 567-581 (10.1007/s11082-010-9362-6)
- [35]. G. -E. Chang, C. O. Chang: Design of strain-free GeSn/SiGeSn quantum-well electroabsorption modulators at 1550 nm wavelength. [Conference] *IEEE 7th International Conf. on Group IV Photonics*, 87-89 (2010)
- [36]. V. Chakraborty, B. Mukhopadhyay, P. K. Basu: Study of GeSn/SiGeSn RCE photodetectors based on Franz-Keldysh effect and quantum confined Stark effect. [Journal] *Opt. Quant. Electron.* **47**, 2381-2389 (10.1007/s11082-014-9998-8)
- [37]. C. G. Van de Walle, R. M. Martin: Theoretical calculations of heterojunction discontinuities in the Si/Ge system. [Journal] *Phys. Rev. B* **34**, 5621 (10.1103/PhysRevB.34.5621)
- [38]. B. Mukhopadhyay, G. Sen, R. Basu, S. Mukhopadhyay, and P. K. Basu: Prediction of large enhancement of electron mobility in direct gap $\text{Ge}_{1-x}\text{Sn}_x$ alloy. [Journal] *Phys. Status Solidi B*, **254**, 1700244 (10.1002/pssb.201700244)
- [39]. K. Kishino, M. S. Unlu, J. -I. Chyi, J. Reed, L. Arsenault, H. Morkoc: Resonant Cavity-Enhanced (RCE) photodetectors. [Journal] *IEEE J. Quant. Electron.* **27**(8), 2025-2034 (10.1109/3.83412)
- [40]. H. A. Khan: Spectral Response Modeling and Analysis of Heterojunction Bipolar Phototransistors. [Ph. D Thesis] *The University of Manchester* (2010)
- [41]. V. Chakraborty, B. Mukhopadhyay, P. K. Basu: Performance prediction of an electro absorption modulator at 1550 nm using GeSn/SiGeSn Quantum Well structure. [Journal] *Phys. E: Low-dimensional Systems and Nanostructures* **50**, 67-72 (10.1016/j.physe.2013.02.023)